Beam shaping profiles and propagation

David L. Shealy[a] and John A. Hoffnagle[b]

[a] University of Alabama at Birmingham, Department of Physics,
1530 3rd Ave. S, Birmingham, AL 35294-1170
[b] IBM Almaden Research Center,
650 Harry Road, San Jose, CA 95120-6099

ABSTRACT

A number of flattened irradiance distributions have been proposed and analyzed in the literature, including the super-Gaussian, flattened-Gaussian, Fermi-Dirac, and super-Lorentzian as well as generalizations of these functions to include multiple shape parameters. Previous work has made comparisons between these different families of functions and examined the effects of propagation (diffraction) on the shape of the beam profile. In this paper, we examine the normalization of different functions, comparisons of profile shapes using different parameters within each family, the slope of the profiles at the half-height point of the irradiance, and two conditions that permit matching shapes of profiles from different families. Then, we summarize the results of diffraction for variation of the profile shape parameters, beam propagation, and diameter of the exit aperture on the shape of a beam as it leaves the optics. Results are also presented which identify the regions and amounts of aspheric surface sag that is required to produce a flattened beam profile as compared to a top-hat profile profile.

Keywords: laser beam shaping, profiles, propagation, optical design

1. INTRODUCTION

Aspheric optics were proposed by Kreuzer[1,2] in 1964 for use in lossless laser beam shaping with a pair of plano-aspheric lenses, whose surface contours are determined by imposing the geometrical optics law of intensity and the constant optical path length condition between the input and output beams. Since lossless beam shaping requires use of aspheric optics, there was an interlude of thirty years from the first proposal to use a pair of plano-aspheric lenses for shaping a Gaussian beam into a uniform irradiance beam to the first publication of experimental results by Jiang, Shealy, and Martin,[3,4] using a pair of plano-aspheric lenses which were diamond-turned in CaF_2 in a Galilean configuration, as shown in Fig. 1(a).

Since the shape of the output beam is affected by the finite size of the beam shaper apertures and by propagation of the beam,[5] Kasinski and Burnham[6] calculated the phase distortion introduced by the first plano-aspheric lens that is required to transform a Gaussian beam into a more uniform beam with a super-Gaussian irradiance profile. From the phase distribution required for this beam shaping transformation, the sag of an aspheric lens surface was computed by multiplying the phase times the laser wavelength and dividing by the lens index of refraction minus one. This beam shaping lens surface was diamond-turned in CaF_2. A second beam shaping lens with negative phase of the first lens was also fabricated to create a collimated output beam with the transformed super-Gaussian output beam.

Hoffnagle and Jefferson[7,8] describe an optical system that transforms a laser beam with an axially-symmetric irradiance profile into a beam with a different axially-symmetric profile with continuous, sigmoidal irradiance distribution, such as a Fermi-Dirac distribution. The design method of Kreuzer was used to determine sag of aspheric surfaces in a Keplerian configuration, as shown in Fig. 1(b). Hoffnagle and Jefferson have analyzed the optical systems for shaping an input Gaussian beam into a Fermi-Dirac output beam profile and have shown that the Fermi-Dirac function has similar behavior as the super-Gaussian function. Hoffnagle and Jefferson provide

Further author information:
D.L.S.: E-mail: dls@uab.edu, Tel.: 205-934-8068
J.A.H.: E-mail: hoffnagl@almaden.ibm.com, Tel.: 408-927-1137

detailed characterization of a refractive beam shaper at 514nm, which shows that the output beam irradiance variation is less than 5% and that the rms variations of the OPD over the beam is 13nm, and have also shown that the flexibility of the two-lens beam shaper is enhanced by its insensitivity to wavelength (deep-UV to near-IR) and by the large depth of field of the output beam.

To avoid diffraction effects in regions of sharp changes in the irradiance, several analytic functions with a uniform central region and a continuous variation from the uniform region to the almost null region have been studied and reported in the literature. In this work, we consider four specific flattened beam profiles: the super-Gaussian,[9] the flattened-Gaussian,[10] the Fermi-Dirac,[7] and the super-Lorentzian[11] distribution. In Sect. 2, we examine the normalization of the different profile functions, compare profiles with different shape parameters within each family, compare the slope of different profiles at the half-height point of the irradiance, and identify two conditions that permit matching profiles from different families. In Sect. 3, we examine the effect of diffraction for variation of the shape parameters, beam propagation, and the diameter of the exit aperture on the beam as it leaves the optics. In Sect. 4, we examine the requirements placed on the sag of aspheric surfaces to produce a flattened beam profile which propagates well as compared to a top-hat beam.

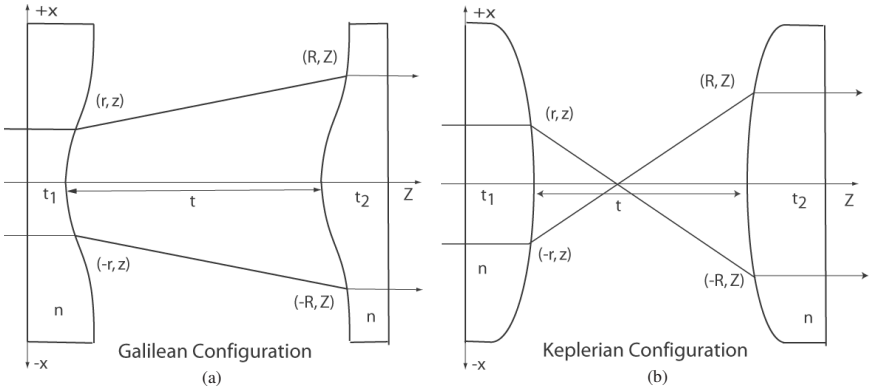

Figure 1. Optical layout of two-lens laser beam shaper in (a) the Galilean configuration and (b) the Kaplerian configuration.

2. IRRADIANCE PROFILES

Consider axially symmetric beams propagating along the z-axis. The input and output irradiance distributions are labelled by $I_{\text{in}}(r)$ and $I_{\text{out}}(R)$, respectively. Ideally, the optical system will not block any power from the beam as a result of the lens apertures. Therefore, we assume that both input and output beams contain the same total power, which is normalized to unity,

$$2\pi \int_0^\infty I_{\text{in}}(r)\, r dr = 2\pi \int_0^\infty I_{\text{out}}(R)\, R dR = 1. \tag{1}$$

The beam profiles are represented by general functions of the spatial coordinates of the aperture and of parameters describing the shape of the functions. Perhaps, the most common beam shaping problem is the transformation of a Gaussian beam into a top-hat beam

$$I_{\text{in,G}}(r) = \left(\frac{2}{\pi w_0^2}\right) \exp\left[-2\left(\frac{r}{w_0}\right)^2\right], \tag{2a}$$

$$I_{\text{out,TH}}(R) = \frac{\text{circ}(R/R_{\text{max}})}{\pi R_{\text{max}}^2}. \tag{2b}$$

where w_0 is the input beam waist, R_{max} labels the radius of the exit aperture of the beam shaper, and $\text{circ}(\text{R}/\text{R}_{\text{max}})$ is equal to unity for $0 \le \text{R} \le \text{R}_{\text{max}}$ and to zero otherwise.

A general flattened output irradiance profile can be written as a product of its normalization constant, $I_0(\sigma, R_0)$, which is determined by requiring the input beam profile to be normalized according to Eq. (1), and its functional dependence $\mathfrak{f}(\sigma, R/R_0)$, which depends on the shape parameter σ and on the ratio of the radial coordinate, R, to the the beam width, R_0, of each distribution:

$$I_{\text{out}}(\sigma, R/R_0) = I_0(\sigma, R_0) \times \mathfrak{f}(\sigma, R/R_0). \tag{3}$$

The width parameter, R_0, defines a length scale over which the profile decreases to some significant value for the specific profile distribution, such as, half or e^{-2} of its axial value. The shape parameter σ specifies the shape of the profile distribution, such as, the power of the radial coordinate of a super-Gaussian profile.

The functions and normalization constants of the Fermi-Dirac, the super-Lorentzian, the super-Gaussian, and the flattened-Gaussian distributions are defined in this section. Explicitly, the Fermi-Dirac function is defined by

$$I_{\text{out,FD}}(\beta, R/R_{FD}) = I_{0,\text{FD}}(\beta, R_{FD}) \left\{1 + \exp\left[\beta\left(\frac{R}{R_{\text{FD}}} - 1\right)\right]\right\}^{-1}, \tag{4}$$

where R_{FD} corresponds to R_0 in Eq. (3) and is the radius at which the output irradiance falls to half of its axial value. β is a dimensionless shape parameter for the Fermi-Dirac function. When β increases, the output profile approaches a more uniform distribution where there is a continuous variation of irradiance from zero to its maximum value on axis. The normalization constant is determined by evaluating Eq. (1) for this distribution and solving for the normalization constant to obtain

$$I_{\text{o,FD}}(\beta, R_{FD}) = \frac{3\beta^2}{\pi R_0^2 \left[3\beta^2 + 6\text{dilog}(1 + \exp(-\beta)) + \pi^2\right]}. \tag{5}$$

The dilogarithm function is also known as Spencer's integral for $n = 2$ and is given by

$$\text{dilog}(x) = \int_1^x \frac{\ln t}{1 - t} dt. \tag{6}$$

Equation (6) can also be expressed as an alternating series[12]

$$\text{dilog}(x) = \sum_{k=1}^{\infty} (-1)^k \frac{(x-1)^k}{k^2} \tag{7}$$

which converges quickly for its use in Eq. (5). Figure 2(a) displays the output irradiance of the Fermi-Dirac function for different shape parameters β. For small β there is a noticeable cusp in the profile on axis. Li[11] proposes that a necessary condition for flat-topped beams is

$$\left[\frac{d^m \mathfrak{f}(r)}{dr^m}\bigg|_{r=0} = 0 \quad \text{for } m = 1, 2, 3, ... \right. \tag{8}$$

where $\mathfrak{f}(r)$ represents an axially symmetric flattened beam profile. Li notes that the super-Gaussian, the flattened-Gaussian, and the super-Lorentzian distributions satisfy Eq. (8), but the Fermi-Dirac does not satisfy this condition for small β . Qualitatively, it follows from Fig. 2(a) that as β becomes larger than ten, the Fermi-Dirac function approaches a circ function, except that the irradiance varies continuously from 0 to the uniform axial value as one moves across the aperture. In the limit as β approaches infinity, one can prove that Eq. (4) approaches the circ distribution, based on evaluating this limit when R/R_{FD} is less than or equal to one or greater than one.

The super-Lorentzian function is defined by

$$I_{\text{out,SL}}(M, R/R_{SL}) = \frac{I_{0,\text{SL}}(M, R_{SL})}{\left[1 + (R/R_{SL})^M\right]}, \tag{9}$$

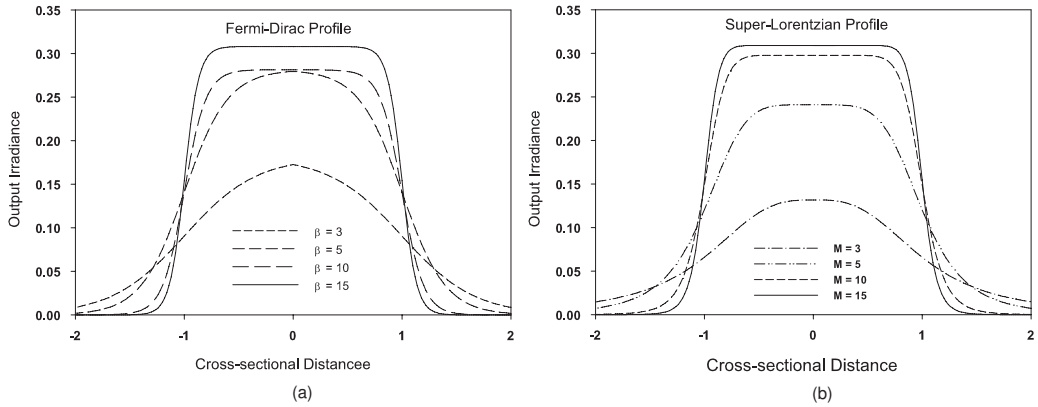

Figure 2. (a) Fermi-Dirac and (b) super-Lorentzian output irradiance for shape parameters β and M. All profiles are normalized such that the total energy contained within each irradiance distribution over all space is equal to unity. The cross-sectional distance is expressed in the normalized units of the beam width.

where R_{SL} is the radius at which the output irradiance falls to half of its axial value, and M is a dimensionless shape parameter for the super-Lorentzian function. When M increases, the output profile approaches a more uniform distribution where there is a continuous variation of irradiance from zero to its maximum value of $I_{0,\mathrm{SL}}(M, R_{SL})$. The normalization constant is determined by evaluating Eq. (1) for this distribution and solving for the normalization constant to obtain

$$I_{0,\mathrm{SL}}(M, R_{SL}) = \frac{M \sin(2\pi/M)}{2\pi^2 R_{\mathrm{SL}}^2}. \tag{10}$$

Figure 2(b) displays the output irradiance of the super-Lorentzian function for different shape parameters M. Qualitatively, it follows from Fig. 2(b) that as M becomes larger than ten, the super-Lorentzian function approaches a circ function, except that the irradiance varies continuously from 0 to the uniform axial value as one moves across the aperture. In the limit as M approaches infinity, one can prove that Eq. (9) approaches the circ distribution, based on evaluating this limit when R/R_{SL} is less than or equal to one or greater than one. From Fig. 2, the Fermi-Dirac and super-Lorentzian have similar shapes for large values of β and M. However, the super-Lorentzian function has a more uniform central region than the Fermi-Dirac function for small values of the respective shape parameters.

The super-Gaussian function is defined by

$$I_{\mathrm{out,SG}}(p, R/R_{SG}) = I_{0,\mathrm{SG}}(p, R_{SG}) \exp\left[-2\left(\frac{R}{R_{SG}}\right)^p\right] \tag{11}$$

where R_{SG} is the radius at which the output irradiance falls to e^{-2} of its axial value, and p is a dimensionless shape parameter for the super-Gaussian function. When p increases, the output profile approaches a more uniform distribution where there is a continuous variation of irradiance from zero to its maximum value of $I_{0,\mathrm{SL}}(M, R_{SG})$. The normalization constant is determined by evaluating Eq. (1) for this distribution and solving for the normalization constant to obtain

$$I_{0,\mathrm{SG}}(p, R_{SG}) = \frac{4^{1/p} p}{2\pi R_{\mathrm{SG}}^2 \Gamma(2/p)}, \tag{12}$$

where $\Gamma(z)$ is the Euler Gamma function.[12] Figure 3(a) displays the output irradiance of the super-Gaussian function for different shape parameters p. Qualitatively, it follows from Fig. 3(a) that as p becomes larger than ten, the super-Gaussian function approaches a circ function, except that the irradiance varies continuously from

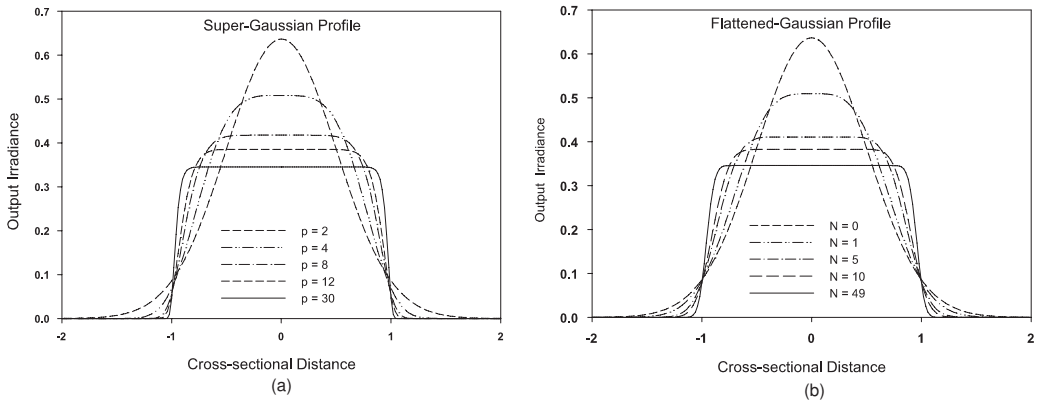

Figure 3. (a) super-Gaussian and (b) flattened-Gaussian output irradiance for shape parameters p and N. All profiles are normalized such that the total energy contained within each irradiance distribution over all space is equal to unity. The profiles for $p = 2$ and $N = 0$ reduce to the Gaussian profile with axial irradiance equal to 0.6366. The axial irradiance of the super-Gaussian profiles with $p = 4, 8, 12, 30$ are equal to $0.5079, 0.4126, 0.3851, 0.3452$, respectively, and of the flattened-Gaussian profile with $N = 1, 5, 10, 49$ are equal to $0.5093, 0.4110, 0.3827, 0.3458$, respectively.

0 to the uniform axial value as one moves across the aperture. In the limit as p approaches infinity, one can prove that Eq. (11) approaches the circ distribution, based on evaluating this limit when R/R_{SG} is less than or equal to one or greater than one.

The flattened-Gaussian function is defined by

$$I_{\mathrm{out,FG}}\left(N, R/R_{FG}\right) = I_{0,\mathrm{FG}}\left(N, R_{FG}\right) \exp\left[-2\left(N+1\right)\left(R/R_{FG}\right)^2\right] \sum_{m,n=0}^{N} \frac{\left[\left(N+1\right)\left(R/R_{FG}\right)^2\right]^{n+m}}{n!m!} \tag{13}$$

where R_{FG} is the radius at which the output irradiance falls to $\Gamma\left(N+1, N+1\right)^2 / \Gamma\left(N+1\right)^2$ of its axial value. N is a dimensionless shape parameter for the flattened-Gaussian function. When $N = 0$, flattened-Gaussian function reduces to the standard Gaussian function given by Eq. (2a) or by the super-Gaussian function displayed by Eq. (11) with $p = 2$. When p increases, the output profile approaches a more uniform distribution where there is a continuous variation of irradiance from zero to its maximum value of $I_{0,\mathrm{FG}}\left(N, R_{FG}\right)$. The normalization constant is determined by evaluating Eq. (1) for this distribution and solving for the normalization constant to obtain

$$I_{0,\mathrm{FG}}\left(p, R_{FG}\right) = \left\{2\pi R_{FG}^2 \sum_{m,n=0}^{N} \left[\frac{2^{(-m-n)}}{4\left(N+1\right)} \begin{pmatrix} m+n \\ n \end{pmatrix}\right]\right\}^{-1}. \tag{14}$$

Figure 3(b) displays the output irradiance of the flattened-Gaussian function for different shape parameters N. Qualitatively, it follows from Fig. 3(b) that as N becomes larger than ten, the flattened-Gaussian function approaches a circ function, except that the irradiance varies continuously from 0 to the uniform axial value as one moves across the aperture. In the limit as N approaches infinity, one can prove that Eq. (13) approaches the circ distribution, based on evaluating this limit when R/R_{FG} is less than or equal to one or greater than one. Santarsiero and Borghi[13] established relationships between the shape parameters of a super-Gaussian and a flattened-Gaussian beam by minimizing the mean squared difference between the profiles of the field amplitudes. Bagini et al.[14] show that the shape parameter p of a super-Gaussian profile is proportional to the square root of the shape parameter N on the flattened-Gaussian distribution for large values of the respective shape parameters.

As a measure of the width and slope of the beam profile within the transition region for different output irradiance distributions, we have made a comparison of the slope at the radial half-height point. That is, the

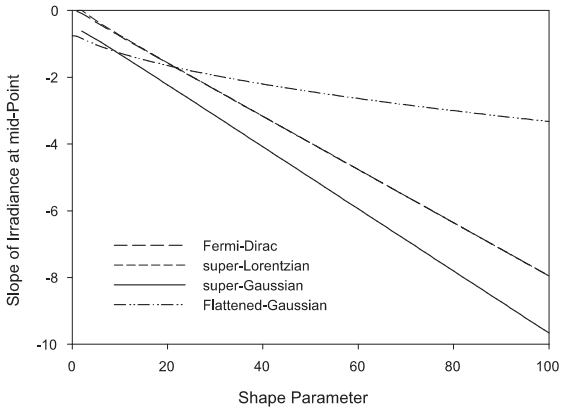

Figure 4. Comparison of the slope of the Super-Lorentzian, Fermi-Dirac, Flattened-Gaussian, and Super-Gaussian distributions at the mid-point, i.e., the radial point at which the relative irradiance distribution is equal to 0.5, as a function of the corresponding shape parameters ranging from 2 to 100.

radial coordinate at which the irradiance is equal to half of its axial value. Figure 4 presents a comparison of the slope of each distribution at the radial half-height point. It follows form Fig. 4 that the slope of the super-Gaussian, super-Lorentzian, and Fermi-Dirac profiles at the half-height point is linearly proportional the the corresponding shape parameter. Whereas, the slope of the flattened-Gaussian distribution has a non-linear dependence on its shape parameter.

From Fig. 4, there is an interesting region of shape parameters ranging from 10-to-20 where each of these profiles can have the same value for the slope of its irradiance at the radius of the half-height point. This suggest that two conditions can be used for matching profiles: (a) equal radius at half-height point and (b) the same slope at the radius of the half-height point. Consider a specific super-Gaussian profile with $p = 11$ and $R_{SG} = 1$. Applying conditions (a) and (b) for matching a Fermi-Dirac function to this super-Gaussian profile leads to the Fermi-Dirac profile parameters $\beta = 15.66$ and $R_{FD} = 0.903$. Figure 5 displays a plot of the radial cross-section of the irradiance of these two specific profiles. From appearances, the super-Gaussian and Fermi-Dirac profiles from Fig. 5 match very well within the transition region. Diffraction calculations described in the next section predict that the propagation characteristics of these two profiles are similar, since the slope of the irradiance profile within the transition region has a significant impact on the distortion of the irradiance due to diffraction.

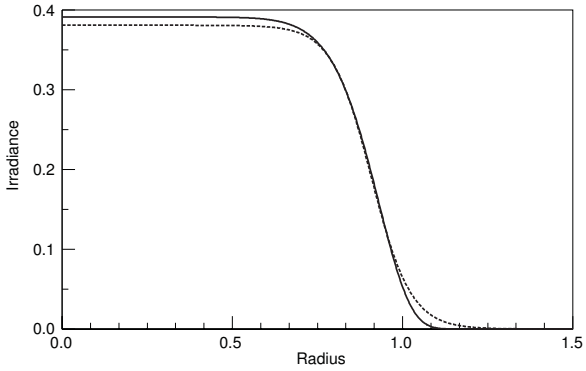

Figure 5. Comparison of a radial cross-section of a Fermi-Dirac profile (broken-line) with $R_{FD} = 0.903mm$ and $\beta = 15.66$ and a Super-Gaussian profile (solid line) with $R_{SG} = 1.0mm$ and $p = 11$.

3. PROPAGATION

As noted earlier, the constant optical path length condition is used to determine the sag of the second aspheric surface to ensure that the output beam is collimated and parallel to the optical axis, while correcting the aberrations introduced by the first aspheric lens in order to reshape the beam irradiance profile. Thus, the second lens generates a *beam* having the desired irradiance profile. In general, diffraction modifies the shaped beam as it propagates from the output aperture. It is well-known that the far-field diffraction pattern of a top-hat profile is the Airy function, and in the far-field limit (Fraunhofer approximation[15]) the other flattened profiles discussed in Sect. 2 evolve to forms similar to the Airy function. It is nevertheless possible to generate an output beam that propagates for a substantial distance without significant distortion due to diffraction. In many applications the usefulness of the beam shaping optics is greatly enhanced if the output beam propagates well. The effects of diffraction on the evolution of the output beam depend on $I_{\rm out}(r)$, and consequently, the choice of a suitable output profile depends on the user's requirements regarding beam propagation.

To calculate the effect of diffraction on the propagating beam we use Kirchhoff's diffraction theory and the Fresnel approximation.[16] Define a quantity $u_0(r)$ which is proportional to the amplitude of the optical field in the output aperture of the beam shaping system,

$$u_0(r) = \sqrt{I_{\rm out}(r)}. \tag{15}$$

After propagating a distance D in the z-direction, the diffracted field is given by the Fresnel-Kirchhoff integral, which for a rotationally symmetric beam can be written[5]

$$u(r,D) = e^{i\varphi}\frac{k}{D}\int_0^{R_{\rm max}} u_0(\rho)\, J_0(k\rho r/D)\, \exp(ik\rho^2/2D)\, \rho\, d\rho, \tag{16}$$

where $k = 2\pi/\lambda$ is the wave number of the light, $R_{\rm max}$ is the radius of the output aperture, $J_0(x)$ is the Bessel function of order 0, and φ is a phase term that includes the oscillations with a period of λ of the phase of the optical wave and the wavefront curvature due to diffraction, but which does not affect the irradiance calculation. It is straightforward to evaluate the Fresnel-Kirchhoff integral numerically. When displaying the results of such calculations, it is convenient to plot the irradiance of the diffracted beam normalized by $I_{\rm out}(0)$. We will refer to this quantity, equal to $|u(r,D)|^2/I_{\rm out}(0)$, as the relative irradiance of the diffracted beam.

Note that since the wavelength λ sets a natural length scale in Eq. (16) the profile of the propagated beam depends on the propagation distance D and the size of the beam R_0. These three lengths can be combined into the dimensionless Fresnel number,

$$N_F = R_0^2/\lambda D, \tag{17}$$

which plays a key role in diffraction theory. For an output beam of a given shape, the shape of the propagated beam depends only on N_F, regardless of the individual values of λ, D, and R_0. This can be seen by introducing scaled transverse coordinates

$$\alpha = R_{\rm max}/R_0 \tag{18}$$

$$\xi = r/R_0 \tag{19}$$

$$\tau = \rho/R_0 \tag{20}$$

as well as functions that express the optical amplitude in terms of the dimensionless, scaled coordinates,

$$v(\xi, N_F) = u(r,D) \tag{21}$$

$$v_0(\tau) = u_0(\rho). \tag{22}$$

Then, Eq. (16) transforms to

$$v(\xi, N_F) = 2\pi N_F e^{i\varphi}\int_0^{\alpha} v_0(\tau)\, J_0(2\pi N_F \xi\tau)\, \exp(i\pi N_F \tau^2)\, \tau\, d\tau. \tag{23}$$

This equation relates the shape of the propagated beam to the original beam shape and N_F.

To illustrate the effect of beam shape on propagation, we examine the dependence of uniformity of the irradiance profile on the beam profile shape parameter, the axial distance of propagation from the output aperture, and the radial size of the output aperture. Figure 6 shows the relative irradiance over a plane perpendicular to the optical axis at a distance of 1 m from the output aperture for three Fermi-Dirac profiles that differ only in the beam shape parameter, β. The beam radius in both cases is $R_0 = 3.0$ mm, $R_{\max} = 5.0$ mm, and the wavelength is $\lambda = 532$ nm. To obtain the propagated profile, Eq. (16) was evaluated with $R_{\max} = 5$ mm. One sees that the more rounded beam show in plot (a) with $\beta = 15$, propagates for 1 m with not apparent ripples due to diffraction, while the more steep-sided beam as shown in plots (b) and (c), with $\beta = 50, 100$ have approximately 25 - 40% of ripples after 1 m. Figure 6 establishes that a Fermi-Dirac profile with $\beta = 15$ will propagate 1 m with minor distortion of the profile from diffraction.

Figure 7 displays the relative irradiance over a plane for a Fermi-Dirac beam with $\beta = 15$, $R_0 = 3.0$ mm, $R_{\max} = 5$ mm, and $\lambda = 532$ nm after propagating (a) 1 m, (b) 2 m, and (c) 4 m. After the beam propagates 2 m, there are distortions from uniformity of approximately 10 %, and the beam is unrecognizable as a flattened beam after 3 m of propagation. Similar studies have been published for super-Gaussian[17] and flattened Gaussian[14] profiles. In all cases, the calculations show that the more nearly the flattened beam resembles a top-hat, the more drastic are the effects of diffraction on the irradiance profile as the beam propagates.

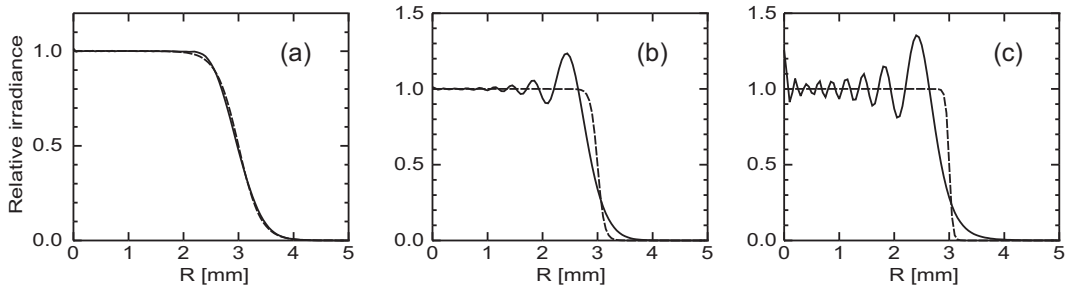

Figure 6. Propagation of Fermi-Dirac beams with $R_0 = 3.0$ mm, $R_{\max} = 5.0$ mm, and $\lambda = 532$ nm, $D = 1$ m,$N_F = 16.9$, and $\beta = 15, 50$, and 100 in plots (a) –(c), respectively. On each plot, the broken curve shows the original profile without any distortion as a result of diffraction.

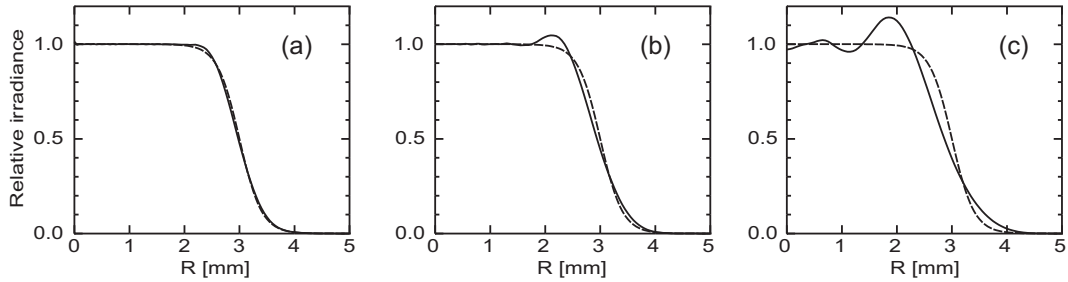

Figure 7. Propagation of Fermi-Dirac beams with $R_0 = 3.0$ mm, $R_{\max} = 5.0$ mm, and $\lambda = 532$ nm. Plots (a)–(c) show the propagation of a beam with $\beta = 15$ and (a) $D = 1$ m, $N_F = 16.9$; (b) $D = 2$ m, $N_F = 8.5$; (c) $D = 4$ m, $N_F = 4.2$.

Another important dimensional parameter in Eq. (16) is the radius of the output aperture, $R_{\max}$. With the exception of the top-hat profile, the output profiles discussed in Sect. 2 are of infinite extent, so for systematic studies of the effect of profile *shape* on propagation, one should choose the upper limit of integration in Eq. (16) to be large enough so that truncation effects are negligible, as was done for the calculations summarized in Figs. 6 and 7 above. Real lenses, however, are of finite size and in fact the designer of practical beam shaping optics will generally try to keep the lens diameters as small as possible, because it is expensive to figure and test aspheric surfaces. In this case, finite aperture effects are important, and they are especially pronounced for beams with

rotational symmetry.[18] If propagation issues are of concern, then one should evaluate Eq. (16) with the design value of $R_{\max}$, to insure that the effect of the finite aperture is properly taken into account. The importance of the output aperture is illustrated in Fig. 8, which shows how the relative irradiance of a Fermi-Dirac beam with $\beta = 15$ and $R_0 = 3.0$ mm that propagates for 1 m with $\lambda = 532$ nm (corresponding to $N_F = 16.9$) depends on the choice of the output aperture. The effect of a finite output aperture can be significant, even though the aperture intercepts only a small fraction of the energy in the beam. For the parameters of this beam, at a radius of 4.0 mm the irradiance has fallen to 2.4% of its value on the beam axis, and the aperture transmits over 99% of the total beam energy; but still diffraction from the aperture has a pronounced effect on the propagated beam, as can be seen from Fig. 8(b).

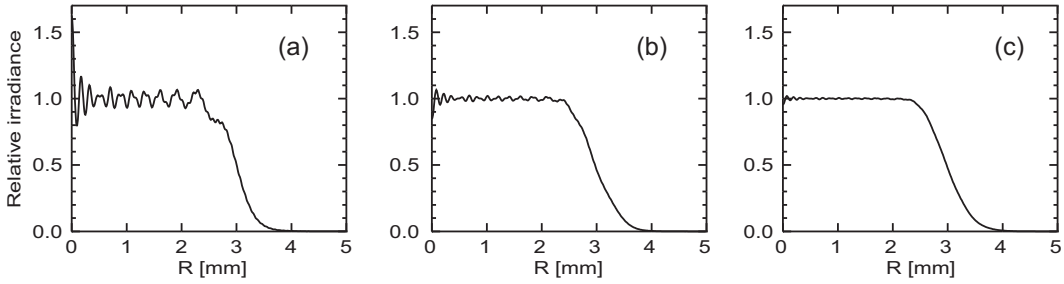

Figure 8. Effect of finite output aperture on the propagation of a Fermi-Dirac beam with $R_0 = 3.0$ mm and $\beta = 15$. The curves show relative irradiance for $\lambda = 532$ nm are propagation distance $D = 1$ m, corresponding to $N_F = 16.9$. The output aperture is (a) $R_{\max} = 3.5$ mm; (b) $R_{\max} = 4.0$ mm; (c) $R_{\max} = 4.5$ mm

The systematic study of beam propagation effects is complicated by the lack of a single, quantitative figure of merit for comparison of the propagation behavior of different beams. Hoffnagle and Jefferson[7] suggested using the range over which the beam propagates, while still satisfying predetermined conditions (essentially user-specified tolerances) on efficiency and uniformity of the propagated irradiance profile. The optical amplitude plays a more fundamental role in diffraction theory than the irradiance, and recognizing this Borghi, Gori, Santarsiero, and Vicalvi have introduced concepts of shape-invariance error[19] and shape-invariance range[20] based on the deviation of the amplitude from a nominal form. However, experimentally it is considerably more difficult to measure the field amplitude than the irradiance.

One figure of merit for beam propagation which has found widespread acceptance is Siegman's M^2 parameter.[21] It has been expressed analytically for the super-Gaussian[17] and flattened Gaussian[14] profiles and shown that M^2 increases monotonically with the shape parameters of these profiles. This means that the propagation range of a flattened beam profile decreases. The more steeply the edges of the beam roll off, the larger M^2 becomes, and in the limit of infinite beam shape parameter, for which the profile approaches a top-hat, M^2 diverges. Studies of the M^2 dependence and of the Fresnel-Kirchhoff integral both illustrate the same basic point: that in the design of beam shaping optics there is a trade-off to be made between achieving a beam with simultaneously large uniformity and efficiency, and one that propagates well. A gradual roll-off at the edge of the beam is necessary for long propagation range, and this implies that the beam shape parameter cannot be chosen to be arbitrarily large. In addition, we have seen that for a practical design it is important to be aware of the effect of finite aperture on the propagation of the shaped beam.

4. ASPHERIC SURFACE SAG

The optical design of the aspheric surfaces of a refractive laser beam shaper, such as, shown in Fig. 1 was first described by Kreuzer,[1,2] who used the geometrical optics law of intensity and the constant optical path length condition between the input and output beams to obtain an integral express for the sag of each aspheric surface. Jiang, Shealy, and Martin,[3,4] and Hoffnagle and Jefferson[7,8] have used the same principles for design of plano-aspheric beam shapers which were built and tested. The references given in this paragraph provide sufficient description of how to compute the sag of a refractive laser beam shaper.

Figure 9 presents a comparison of the difference in the sag of the first and second aspheric surfaces of a beam shaper designed to transform a Gaussian input beam into a Fermi-Dirac profile with the sag of beam shapers designed to transform the Gaussian beam into a top-hat profile and into a super-Gaussian profile. The beam shaper lens spacing is 150 mm, and the index of refraction is 1.460706, corresponding to fused silica at 532 nm. The input Gaussian beam has a waist of $w_0 = 3.0$ mm, and the input aperture is $r_{max} = 4.0$ mm. The output Fermi-Dirac profile has a shape parameter of $\beta = 15.66$, which is the same as used in Fig. 5; the super-Gaussian beam has a shape parameter of $p = 11$; and the corresponding output beam widths are: $R_{FD} = 3.0$ mm, $R_{TH} = 3.0$ mm, and $R_{SG} = 3.322$ mm.

These results suggest that the sag of the outer region of aspheric surfaces is responsible for producing an output profile with a gradual slope of the irradiance profile from its central uniform region to the null region. It is also interesting to note that 90% of the total beam energy is encircled within an input aperture radius of $r = 2.35$ mm over the first aspheric surface. For this radius, the deviation of the sag curves is equal to 0.44 μm for the Fermi-Dirac to super-Gaussian profile comparison and 0.95 μm for the Fermi-Dirac to top-hat profile comparison. Each of these profiles have the same radius of the half-height. Also, the difference in sag of the aspheric surface for central region of each profile are approximately the same, while the sag of the outer region of aspheric surfaces is responsible for creating a profile that propagates well. These results suggest that the local aspheric figure error for the outer region of the lenses should be less than the difference between the sag of Fermi-Dirac and super-Gaussian profiles, since these beams have similar propagation characterizes.

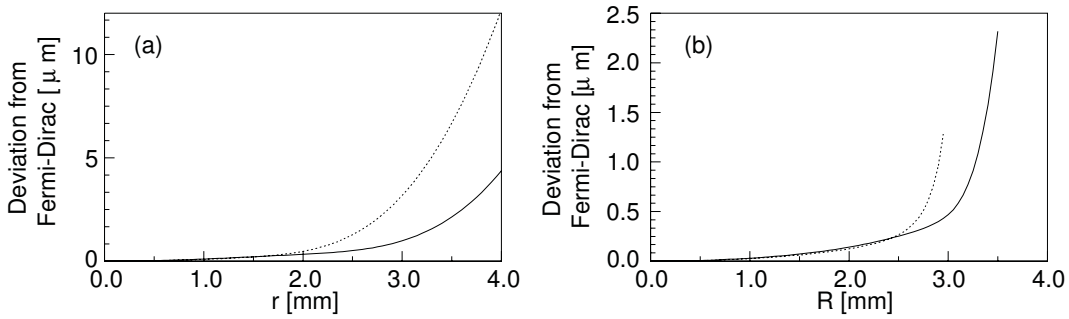

Figure 9. (a) Difference in sag of the first aspheric surface designed for Fermi-Dirac output profile with the sag of beam shapers designed for the top-hat profile (broken line) and the super-Gaussian profile (solid line). (b) Difference in sag of first aspheric surface designed for Fermi-Dirac output profile with the sag of beam shapers designed for the top-hat profile (broken line) and the super-Gaussian profile (broken line).

5. CONCLUSION

Methods and results are presented for computing four families of flattened irradiance profiles, including the Fermi-Dirac, super-Lorentzian, super-Gaussian, and flattened-Gaussian functions. In each case, the total power over a plane of infinite extent has been normalized to unity, which has been used to determine normalization constants for each irradiance profile. It has been proposed that irradiance profiles from different families of functions match when the radius at half-height and the slope of the irradiance at the radius of half-height are equal for each profile. Kirchhoff diffraction theory has been used to study the effects of profile shape parameters, propagation, and diameter of output aperture on the uniformity of irradiance. A gradual roll-off of irradiance from a uniform central region increases the distance from the output aperture that a beam can propagate while there is limited deviation from a uniform irradiance beam. Overall, diffraction calculations show that in the design of laser beam shaping optics there is a trade-off to be made between achieving a beam with simultaneously large uniformity and efficiency, and one that propagates will. In addition, it has been shown that for a practical design it is important to be aware of the effect of finite aperture on the propagation of the shaped beam, where results suggest that the diameter of the output aperture should be about 30% larger than the beam width. Finally, it has been shown that the gradual roll-off of a flattened beam is controlled by the outer annular region of width of about one-third of the radius of the lens aperture, which requires figure errors less than a wavelength.

REFERENCES

1. J. Kreuzer, "Laser light redistribution in illuminating optical signal processing systems," in *Optical and Electro-Optical Information Processing*, J. T. Tippett, D. A. Berkowitz, L. C. Clapp, C. J. Koester, and J. Alexander Vanderburgh, eds., p. 365, (Cambridge, MA), 1965.
2. J. L. Kreuzer, "Coherent light optical system yielding an output beam of desired intensity distribution at a desired equiphase surface," *US Patent* **3,476,463**, 4 November 1969.
3. W. Jiang, D. L. Shealy, and J. C. Martin, "Design and testing of a refractive reshaping system," in *Current Developments in Optical Design and Optical Engineering III*, R. E. Fischer and W. J. Smith, eds., *Proc. SPIE* **2000**, pp. 64–75, 1993.
4. W. Jiang and D. L. Shealy, "Development and testing of a refractive laser beam shaping system," in *Laser Beam Shaping*, F. M. Dickey and S. C. Holswade, eds., *Proc. SPIE* **4095**, pp. 165–175, 2000.
5. J. P. Campbell and L. G. DeShazer, "Near fields of truncated-gaussian apertures," *J. Opt. Soc. Am.* **59**, pp. 1427–1429, 1969.
6. J. J. Kasinski and R. L. Burnham, "Near-diffraction-limited laser beam shaping with diamon-turned aspheric optics," *Opt. Lett.* **22**, pp. 1062–1064, 1997.
7. J. A. Hoffnagle and C. M. Jefferson, "Design and performance of a refractive optical system that converts a gaussian to a flattop beam," *Appl. Opt.* **39.30**, pp. 5488–5499, 2000.
8. J. Hoffnagle and C. Jefferson, "Refractive optical system that converts a laser beam to a collimated flat-top beam," *US Patent* **6,295,168**, 25 September 2001.
9. S. D. Silvestri, P. Laporta, V. Magni, O. Svelto, and B. Majocchi, "Unstable laser resonators with super-gaussian mirrors," *Opt. Lett.* **13.3**, pp. 201–203, 1988.
10. F. Gori, "Flattened gaussian beams," *Opt. Commun.* **107**, pp. 335–341, 1994.
11. Y. Li, "Light beams with flat-topped profiles," *Opt. Lett.* **27.12**, pp. 1007–1009, 2002.
12. "Handbook of mathematical functions," *National Bureau of Standards, Applied Mathematics Series, No. 55*, (Washington, D.C. 20402), November 1967. Eq. 27.7.2.
13. M. Santarsiero and R. Borghi, "Correspondence between super-gaussian and flattened gaussian beams," *J. Opt. Soc. Am. A* **16.1**, pp. 188–190, 1999.
14. V. Bagini, R. Borghi, F. Gori, A. Pacileo, M. Santarsiero, D. Ambroshini, and G. Schirripa-Spagnolo, "Propagation of axially symmetric flattened gaussian beams," *J. Opt. Soc. Am. A* **13.7**, pp. 1385–1394, 1996.
15. J. Goodman, *Introduction to Fourier Optics*, McGraw-Hill Book Company, San Francisco, CA, 1968.
16. M. Born and E. Wolf, *Principles of Optics*, Cambridge University Press, Cambridge, UK, seventh ed., 1999.
17. A. Parent, M. Morin, and P. Lavigne, "Propagation of super-gaussian field distributions," *Opt. Quantum Electron.* **24**, pp. S1071–S1079, 1992.
18. A. Siegman, *Lasers*, University Science Books, Mill Valley, CA, 1986.
19. S. Vicalvi, R. Borghi, M. Santarsiero, and F. Gori, "Shape-invariance error for axially symmetric light beams," *IEEE J. Quant. Electr.* **QE-34**, pp. 2109–2116, 1998.
20. F. Gori, S. Vicalvi, M. Santarsiero, and R. Borghi, "Shape-invariance range of a light beam," *Opt. Lett.* **21**, pp. 1205–1207, 1996.
21. A. E. Siegman, "New developments in laser resonators," in *Optical Resonators*, D. A. Holmes, ed., *Proc. SPIE* **1224**, pp. 2–14, 1990.